Geophysical Research Letters

RESEARCH LETTER
10.1029/2021GL097231

Consistent Trends in Dry Spell Length in Recent Observations and Future Projections

Caroline M. Wainwright[1,2], **Richard P. Allan**[1,3], **and Emily Black**[1,2]

[1]Department of Meteorology, University of Reading, Reading, UK, [2]National Centre for Atmospheric Science (NCAS), Reading, UK, [3]National Centre for Earth Observation (NCEO), Reading, UK

Key Points:

- Recent trends in dry spell length during the dry season are consistent with future projections
- Recent trends over South America and West Africa reflect a mix of natural and human caused drivers
- Longer dry spells over north-east South America linked with a warmer North Atlantic Ocean

Supporting Information:

Supporting Information may be found in the online version of this article.

Correspondence to:

C. M. Wainwright,
c.wainwright@imperial.ac.uk

Citation:

Wainwright, C. M., Allan, R. P., & Black, E. (2022). Consistent trends in dry spell length in recent observations and future projections. *Geophysical Research Letters*, *49*, e2021GL097231. https://doi.org/10.1029/2021GL097231

Received 30 NOV 2021
Accepted 21 MAY 2022

Author Contributions:

Conceptualization: Caroline M. Wainwright, Richard P. Allan, Emily Black
Data curation: Caroline M. Wainwright
Formal analysis: Caroline M. Wainwright
Funding acquisition: Emily Black
Investigation: Caroline M. Wainwright, Richard P. Allan, Emily Black
Methodology: Caroline M. Wainwright, Richard P. Allan, Emily Black
Project Administration: Emily Black
Software: Caroline M. Wainwright
Supervision: Richard P. Allan, Emily Black
Visualization: Caroline M. Wainwright
Writing – original draft: Caroline M. Wainwright, Richard P. Allan, Emily Black

Abstract We identify global observed changes in dry-spell characteristics that are consistent with future projections and involve common physical drivers. Future projections of longer dry spells in the dry season increase vegetation water stress and can negatively impact perennial vegetation. Lengthening dry season dry spells of up to ~2 days per decade over South America and southern Africa and shortening of similar magnitude over West Africa display a qualitatively consistent pattern to future projected changes under the Shared Socioeconomic Pathway 2-4.5 intermediate greenhouse gas emissions scenario. By combining a range of present-day climate model experiments, recent trends are linked with both natural and human-caused drivers. Longer dry season dry spells over South America are associated with relative warming of North Atlantic sea surface temperatures and amplified warming over land compared with adjacent oceans; both of which are projected to continue under further warming, suggesting a common driver for recent trends and future projections.

Plain Language Summary Continued warming of climate will further intensify dry seasons which may damage crops and forests. We combine observations and simulations to see if future signals of climate change are already beginning to occur and why. Lengthening dry spells over South America and southern Africa and shorter dry spells over West Africa are found to be consistent with future climate change. In particular, the recent trend of longer dry spells in the dry season over South America is linked with stronger warming over land than over the South Atlantic Ocean and the pattern of warming in the North Atlantic. These effects will become larger as the climate continues to warm, causing the dry season to become more intense over South America.

1. Introduction

Warming of climate is intensifying the global water cycle, strengthening contrasts between wet and dry seasons and increasing the intensity while decreasing the frequency of sub-seasonal precipitation (Allan et al., 2020; Konapala et al., 2020; Liu & Allan, 2013; Schurer et al., 2020). Regionally, changes in atmospheric circulation, including but not limited to the position of the tropical rain belt, also alter the location of the wettest and driest regions and the timing of the seasons (Mamalakis et al., 2021). Rainfall timing and frequency are important in affecting vegetation growth (e.g., Zhang et al., 2018) and more frequent prolonged dry spells have the potential to cause significant detrimental impacts on agriculture and food security, as well as fire risk (Burton et al., 2021). When coupled with higher temperatures and increased evaporative demand under climate change (Greve & Seneviratne, 2015; Padrón et al., 2020; Vicente-Serrano et al., 2020), more intense dry spells can lead to a reduction in soil moisture and increased water stress on vegetation, potentially reducing crop yields and negatively impacting other vegetation. For a given amount of precipitation, more intense but less frequent rainfall has also been linked with reduced soil moisture and above-ground plant productivity, even where mean precipitation is unchanged, based on novel field experiments (Slette et al., 2021). However, the impact of dry spells is also determined by their timing in the seasonal cycle; prolonged dry spells during the dry season may have detrimental impacts on perennial species, including forest vegetation (McDowell et al., 2018). Furthermore, dry season rainfall has been found to have a stronger influence on tropical tree growth than wet season rainfall, with drier dry seasons leading to less tree growth (Zuidema et al., 2022).

Examining projected changes in the length of wet and dry spells across the global tropics, Wainwright et al. (2021) identified longer and more intense dry spells during the annual dry season. While this may limit the impact on crops grown solely during the wet season, it can significantly impact perennial crops, including cocoa. Some of

Writing – review & editing: Caroline M. Wainwright, Richard P. Allan, Emily Black

the largest changes occur in northern South America (Wainwright et al., 2021), a region that produces much of the world's cocoa (Wood & Lass, 2008). A range of observations indicates a decrease in September to November precipitation and river discharge following a long dry season in the southern Amazon associated with a poleward shift in the South Atlantic convergence zone (Correa et al., 2021; Espinoza et al., 2019; Zilli et al., 2019).

Identifying observed changes in dry-spell characteristics that involve common physical drivers and are consistent with future projections contributes toward establishing robustness in these future responses. It is "virtually certain" that since the 1950s the frequency and intensity of heavy precipitation events have increased, across most land regions (Fischer & Knutti, 2016). However, trends in consecutive dry days (CDD) are not coherent over the global land during the 1980-2010 period based on multiple climate models and reanalysis datasets (Sillmann, Kharin, Zhang, et al., 2013), though spatial means across all land grid points may smooth over contrasting regional trends (Wainwright et al., 2021). For example, Cerón et al. (2021) and Avila-Diaz et al. (2020) found an increase in the length of dry spells over the northern La Plata Basin and Brazil, respectively, from the early 1980s to the late 2010s and New et al. (2006) found a statistically significant increase in dry spell duration over southwest Africa over 1961-2000.

Given the urgency for establishing effective adaptation strategies to climate change, it is important to further characterize changes in subseasonal precipitation characteristics such as dry spell length, establish links with driving mechanisms, and attribute causal factors, for future projections. In the present study a recently developed methodology is used to identify changes in mean dry spell length during a dynamically determined dry season that are qualitatively consistent and exhibit similar spatial patterns globally with future projections as documented by Wainwright et al. (2021). We exploit a range of observations (including satellite-based precipitation datasets and reanalysis) and global climate model simulations. These include targeted simulations to enable attribution of changes to different drivers, to investigate whether recent trends result from natural or anthropogenic drivers, and to what extent common mechanisms explain current and future changes.

2. Data and Methodology

2.1. Climate Model Data

Daily precipitation data from *historical* experiments applying realistic radiative forcings over the recent past and future projections following the Shared Socioeconomic Pathway 2-4.5 (SSP245) scenario were extracted from 20 models (Table S1) contributing to Phase 6 of the Coupled Model Intercomparison Project (CMIP6) (Eyring et al., 2016; O'Neill et al., 2016). The *historical* simulations were considered over the period 1 January 1985–31 December 2014, both for looking at recent trends and as a reference period when calculating projected future changes. The SSP245 scenario was used for 1 January 2070–31 December 2099; this is a medium greenhouse gas emissions scenario, producing a radiative forcing of approximately 4.5 W m^{-2} in 2100 (O'Neill et al., 2016). Daily precipitation and surface air temperature as well as monthly sea surface temperature data are used.

Daily precipitation from atmosphere-only (*amip*) simulations, produced as part of CMIP6, were used from 20 models over the period 1 January 1985–31 December 2014. These simulations use the same model setup as the coupled *historical* simulations, but apply observed sea surface temperatures (SSTs) and sea ice so therefore depict realistic internal climate variability, albeit neglecting the direct effects of air-sea coupling.

Detection and Attribution Model Intercomparison Project (DAMIP, part of CMIP6) simulations (Gillett et al., 2016) were also considered to enable the attribution of changes to different drivers. Three DAMIP experiments are considered: *hist-nat*, *hist-GHG*, and *hist-aer*. The *hist-nat* simulations resemble the *historical* simulations, but contain only natural forcings (solar irradiance, volcanic eruptions), with no anthropogenic forcings (anthropogenic aerosol, greenhouse gases). Also considered (in Supplementary Information) were the *hist-GHG* and *hist-aer* experiments which resemble the *historical* simulations, but are forced by changes in greenhouse gases only (*hist-GHG*) or forced by changes in aerosol forcing only (*hist-aer*). Daily precipitation was only available from 10 DAMIP models. Again, only daily precipitation data are used.

2.2. Observational Data

CHIRPS (Climate Hazards group Infrared Precipitation with Stations) global daily precipitation data use thermal infrared imagery, gauge data, a monthly precipitation climatology (CHPClim) and CFS version 2 reanalysis fields

to produce rainfall estimates (Funk et al., 2015) over 50°S-50°N from 1 January 1981 until present. CHIRPS has been used and verified over South America (Paredes-Trejo et al., 2017; Rivera et al., 2018), Africa (Dembélé & Zwart, 2016; Dinku et al., 2018; Toté et al., 2015) and Asia (Bai et al., 2018; Gupta et al., 2020), and exhibits good agreement with other observational datasets. In a recent global assessment, Shen et al. (2020) found that CHIRPS precipitation estimates agree well with Global Precipitation Climatology Center precipitation data over the United States, Europe, Africa, Australia, and South America.

The Multi-Source Weighted-Ensemble Precipitation (MSWEP) dataset was also considered for comparison with CHIRPS. MSWEP is a new global precipitation dataset, available at 3-hourly resolution from 1979 to 2017 (Beck et al., 2019). It combines gauge, satellite, and reanalysis-based data using a methodology that takes advantage of the relative strengths of each data source (Beck et al., 2019).

Also considered is daily precipitation from the fifth generation European Center for Medium-Range Weather Forecasts (ECMWF) atmospheric reanalysis of the global climate (ERA5) which combines large amounts of historical observations into global estimates using advanced modeling and data assimilation (Hersbach et al., 2020). Although precipitation retrievals are only explicitly assimilated over parts of North America, assimilation of a range of meteorological variables combined with high-resolution modeling ensures a realistic representation of large-scale precipitation fields, as evidenced by evaluation against Tropical Rainfall Measuring Mission (TRMM) and Global Precipitation Measurement (GPM) mission's Integrated Multisatellite Retrievals (IMERG) observations (Hersbach et al., 2020; Watters et al., 2021). Monthly surface temperature, dewpoint temperature, evaporation, mean sea level pressure, and the upper layer (level 1) volumetric soil water were also used. Surface (2 m) specific and relative humidity are not available from ERA5; thus they were calculated using surface dewpoint temperature, surface air temperature, and mean sea level pressure.

All three precipitation datasets were considered over 50°S-50°N for 1985-2014 since observational datasets are likely to be less reliable in the early-1980s due to gaps in the satellite records (Funk et al., 2015), and to be comparable with the CMIP6 *historical* simulations. The aim here is to focus on regions with a well-defined annual wet and dry season, thus the mid-high latitudes, where rainfall seasonality is less well-defined were excluded, as in Wainwright et al. (2021).

Observed SSTs (1985-2014) were taken from monthly HadISST (v1.1) data (Rayner et al., 2003). The Atlantic Multi-Decadal Oscillation (AMO) index is obtained from (Trenberth et al., 2021) and based on Trenberth and Shea (2006). The El Niño Southern Oscillation (ENSO) index is taken from the Climate Prediction Center Oceanic Niño Index (https://origin.cpc.ncep.noaa.gov/products/analysis_monitoring/ensostuff/ONI_v5.php) and is defined as 3 months running mean of SST anomalies in the Niño 3.4 region (5°N-5°S, 120°-170°W).

2.3. Dry Spell Calculation

The mean length of dry spells calculation is described by Wainwright et al. (2021). The methodology has three steps: firstly, the seasonality regime at each point is classified into one of four seasonality classes (wet-year-round, dry-year-round, one wet season per year, or two wet seasons per year) using relative entropy (Feng et al., 2013; Pascale et al., 2016) and harmonic analysis (Dunning et al., 2016; Liebmann et al., 2012). The relative entropy quantifies how different the observed annual cycle of rainfall is from a uniform annual cycle with unchanging monthly precipitation; relative entropy is high in regions with a pronounced seasonal cycle, and low in regions with little variation in precipitation throughout the year (Feng et al., 2013; Pascale et al., 2016). Low values of relative entropy were used to determine regions that are wet-year-round, and the driest 20% of grid points were classified as dry-year-round. The remaining grid points were classified as having one or two wet seasons per year using harmonic analysis. Regions, where the amplitude of the second harmonic is larger than the amplitude of the first harmonic, were classified as having two wet seasons per year, whereas regions, where the amplitude of the first harmonic is larger, are classified as having one wet season per year. Here, only grid points with one wet season per year were considered since contrasting trends can occur in separate wet seasons (e.g., East Africa; Tierney et al. [2015]).

Secondly, the method of anomalous accumulation was used to determine the beginning and end dates of the climatological dry (and wet) seasons. The method of anomalous accumulation defines the beginning and end of the wet season as the minima and maxima in the cumulative climatological daily rainfall anomaly. This is computed as climatological mean rainfall for each day of the calendar year minus the annual mean of these daily

totals. The cumulative climatological daily rainfall anomaly is then calculated by summing the climatological daily rainfall anomaly (Dunning et al., 2016; Liebmann et al., 2012). This method is applicable to different datasets (with different biases) at the global scale, since the single parameter used in this methodology is the mean precipitation at that grid point, and thus is specific for each grid point and dataset. Furthermore, other studies have used variants of this methodology to calculate onset dates on a global scale (Bombardi et al., 2019). Seasonality classifications and seasonal beginning and end dates are computed separately for each observational product and model. A previous study found that CMIP6 models had a good representation of the seasonality regime and seasonal timing (Figure S2, S3, and S5 in Wainwright et al. [2021]).

Finally, the mean length of dry spells in the dry season was calculated by taking the mean of the length (in days) of all dry spells (of length 2 days or more) during the dry season. A dry spell is defined as a consecutive period of dry days, using a threshold of below 1 mm day^{-1} to define a dry day, as widely used in the calculation of wet and dry spell lengths (Giorgi et al., 2019; Seneviratne et al., 2012; Sillmann, Kharin, Zwiers, et al., 2013). The results may be sensitive to the choice of threshold, as in regions with very dry dry seasons a large proportion of the days may be below this threshold; a lower threshold was not used due to the limitations of satellite-based rainfall datasets and climate models in reliably representing rainfall totals below this threshold. In fact, this choice is expected to be conservative since dry spell length cannot increase further as dry season rainfall reaches zero yet signals of change are detected suggesting they are robust. Additionally, our results show good agreement with other studies (see Section 3, and Figure 2 in Wainwright et al. [2021]).

2.4. Correlations, Trends, and Robustness

Correlations were computed using the Pearson correlation coefficient. Trends were computed using linear regression, and statistical significance was estimated using the Wald test, with the null hypothesis that the slope is zero. Stippling is used to indicate where the correlation/trend is statistically significant at the 10% level (90% confidence level).

For the future projections (Figures 1a, 3e and 4d) robustness across model simulations was determined using a methodology similar to that in Dosio et al. (2019). Projected changes are considered robust if more than 50% of the simulations show a statistically significant change (*t*-test, 10% significance level) of the same sign as the median and, at the same time, more than 70% of them agree on the sign. The probability of more than or equal to 14 out of 20 models (70%) showing one sign by chance is about 6% based on a binomial calculation. Figures 1a, 3e and 4d show regions with robust changes as stippled.

2.5. Land–Sea Contrast Calculation

In order to explore the role of the changing land-sea temperature contrast on drying over South America, relative humidity changes were estimated by assuming that specific humidity over land is determined by specific humidity changes over the adjacent South Atlantic ocean, a region identified as important in supplying moisture to South America during this season (Gimeno et al., 2010).

The method used by Byrne and O'Gorman (2018) to explore the links between land and ocean warming contrasts and changing relative humidity over land was adapted (for full details see Supplementary Information). Here,"-South America" refers to the region of South America of interest, and "South Atlantic" refers to the region of the South Atlantic that supplies moisture to South America during the dry season. The oceanic supply of moisture is determined by changes in specific humidity over the ocean (see Supplementary). Byrne and O'Gorman (2018) scaled this oceanic supply by the ratio of mean specific humidity between land and ocean, which is typically about 0.7, but for the region of study, we find that this ratio is 0.965 so 1.0 is used as a reasonable approximation. This higher ratio may be due to additional moisture sources, including local recycling. The idealized estimates of relative humidity over South America were calculated for each dry season (May-September) by adding the dry season South Atlantic surface specific humidity anomaly (for each of the 30 dry seasons) to the mean South America dry season specific humidity, and dividing by the saturated specific humidity for the South America region dry season.

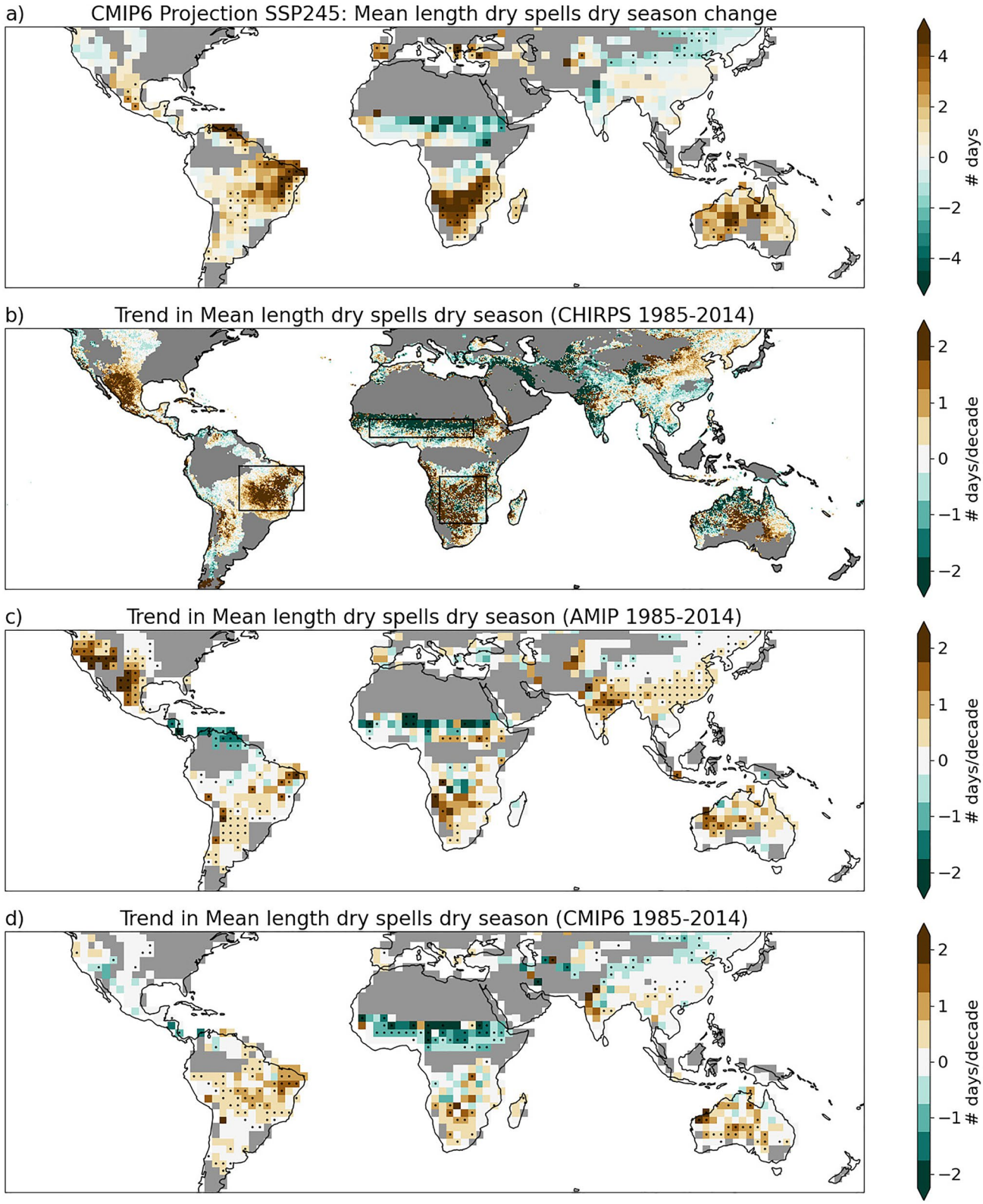

Figure 1.

3. Results

3.1. Recent Trends in Observations and Models

The recently observed trends in the mean length of dry spells in the dry season (Figure 1b) display a qualitatively consistent pattern to future projected changes for the end of the 21st century (Figure 1a) with increases in the mean length of dry spells in the dry season over north-east South America, southern North America, and southern Africa, and decreases over the Sahel; this may suggest that a climate change signal is already being observed over these regions. Increases in dry season dry spell length over north-east South America (of ~2 days per decade) and southern North America are statistically significant and also present in other datasets (Figure 1b, Figure S1). A recent trend of longer dry spells over parts of South America was also found by Avila-Diaz et al. (2020) and Valverde and Marengo (2014). Furthermore, Cerón et al. (2021) found the increase in the length of dry spells over the northern La Plata Basin from 1981 to 2018 was strongest during austral winter (the dry season). Time-series of the mean length of dry spells in the dry season over north-east South America from CMIP6 simulations (Wainwright et al., 2021), which show the transient change, suggest that the increasing trend starts in the early 21st century. This adds to evidence that the observed signal may be linked to climate change. Our study finds a positive trend in southern Africa (Figure 1b). Although not coherent across the region, the trend is consistent with New et al. (2006), which noted an increase in dry spell duration over southwest Africa, using station data over the period 1961-2000. Timeseries showing the transient change of dry season dry spell length over south-east Africa from CMIP6 simulations (Wainwright et al., 2021) show an increasing trend throughout the 21st century, but suggest the emergence of the signal from the noise occurs later than over north-east South America. A decrease in the mean length of dry spells in the dry season over the northern Sahel, observed in CHIRPS is also found in MSWEP and to a lesser extent in ERA5 (Figure 1a, S1), is consistent with Barry et al. (2018), who report a decreasing trend of CDD over West Africa for the period 1981-2010.

To establish if these trends are captured in climate model simulations, and to investigate the driving factors, trends over the recent period (1985–2014) are also calculated using the atmosphere-only (*amip*) and coupled *historical* simulations produced as part of CMIP6 (Figures 1c and 1d). The *amip* simulations include a signal from observed internal climate variability as well as anthropogenic and natural radiative forcings while the ensemble mean of the *historical* simulations primarily contains only the forced component of climate change. Both sets of simulations capture the increase in the mean length of dry spells in the dry season over north-east South America and southern Africa, and the decrease over the Sahel, although the trends are weaker than in the observations. The *amip* simulations capture the increase over southern North America, but this is not captured in the *historical* simulations, which may suggest this is the result of internal (unforced) variability. Both also show an increase in dry spell length over Australia (also seen in future projections, although not statistically significant), which is not seen in CHIRPS (Figure 1a) but is more pronounced in MSWEP and ERA5 (Figure S1). Since MSWEP includes reanalysis data, and ERA5 is a reanalysis dataset, this may suggest that the trend over Australia is related to the model representation of rainfall and drivers over this region (as it is seen in reanalysis and model simulations but not satellite- and ground-based observations).

To determine if these recent trends are solely due to natural forcing agents (volcanic, solar) or whether there is a role of anthropogenic forcing, trends were computed using the *hist-nat* (see methods) simulations produced as part of DAMIP. Three regions were considered (regions shown in Figure 1b); northeast South America, West Africa and the Sahel, and southern Africa.

Over South America (Figures 2a and 2b) the increase in the mean length of dry spells in the dry season is captured by the *amip* and *historical* simulations, but the trend is much weaker (though still positive) in the *hist-nat* simulations (median of 0.15 days/decade across *hist-nat* simulations compared to 0.79 days/decade in *amip* and 1.31 *historical*). This is suggestive that a combination of natural and anthropogenic forcings is responsible for the changes in this region. The distribution of trends for the *hist-nat* simulation is significantly different from the distribution for the *historical* simulations (*t*-test, p value < 0.1), supporting the suggestion of a role of

Figure 1. Recent and future trends in mean length of dry spells in the dry season. (a) Multi-model median future projected change from Coupled Model Intercomparison Project 6 (CMIP6) for 2070-2099 under Shared Socioeconomic Pathway 2-4.5 compared to the *historical* simulation over 1985-2014. Robust changes (see Section 2.4) are stippled. (b) Trend from Climate HazardsGroup Infrared Precipitation with Stations 1985-2014. (c)-(d) Multi-model median trend from *amip* (c) and CMIP6 *historical* (d) simulations over 1985-2014. Gray regions have two wet seasons per year, or are wet or dry year round, as defined in Wainwright et al. (2021). Stippled regions indicate where 70% of the simulations agree on the sign of the trend.

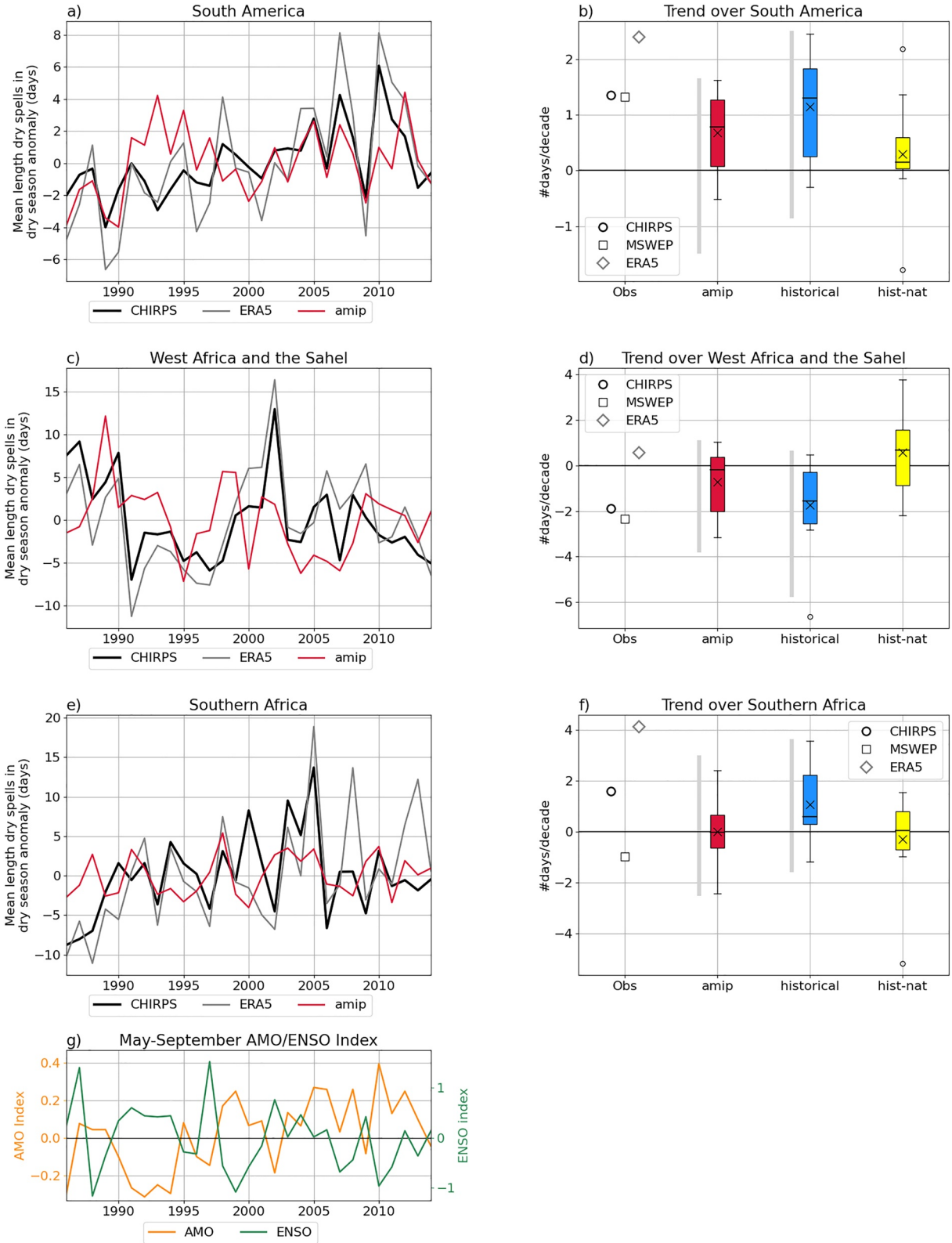

Figure 2.

anthropogenic forcing on this trend. The difference between *amip* and *historical* is not statistically significant; the larger increase in *historical* may be related to elevated warming in the *historical* simulations during this period compared to *amip*. The suppressed global surface warming during some of the period considered (1998-2014) is strongly influenced by an unusual phase of internal climate variability (Kosaka & Xie, 2013) that is therefore not captured by the *historical* simulations ensemble mean which average over their internally generated climate variability. This partially explains why *historical* simulations, on average, exhibit larger surface warming (Mitchell et al., 2020) that may be expected to produce larger associated global water cycle responses.

Over West Africa, the decreasing trend is found only in MSWEP and CHIRPS and is not seen in ERA5. *amip* and *historical* simulations both capture the decreasing trend, which (similarly to South America) is stronger in the *historical* simulations than in *amip*. This may be related to a greater warming trend in coupled *historical* simulations than in observations and simulations driven with prescribed SSTs (i.e., *amip* simulations) since 1979, and particularly over 1998-2014, and relating to internal climate variability that suppressed global warming in this period (Mitchell et al., 2020). However, the *hist-nat* simulations show a range of increasing and decreasing trends, with the mean and median around zero. This therefore also suggests a role of anthropogenic forcing; the *hist-nat* and *historical* distributions are again significantly different (t test, p value < 0.1). Dong and Sutton (2015) concluded that anthropogenic forcings, in particular increases in greenhouse gas concentrations, have been the main factor in the recent recovery in Sahel summer rainfall; our results suggest that anthropogenic forcings have also impacted the dry seasons.

For southern Africa the trend is very different in all three observation datasets (Figure 2, Figure S1-2); the *amip* simulations show weak increasing and decreasing trends, while the *historical* simulations show increasing trends. The *hist-nat* trend distribution is similar to the *amip* trend distribution, but due to the lack of consensus on the observational trend, limited conclusions can be drawn. The *hist-aer* (aerosol only) and *hist-GHG* (greenhouse gas only) simulations were also considered (see Figure S2). However, the model spread was so large that it was difficult to draw conclusions from these simulations, though previous studies have highlighted the important role of Pacific decadal internal climate variability on precipitation over southern Africa (e.g., Cook, 2001; Maidment et al., 2015).

The most robust trends in dry season dry spell length across the observations and *amip* and *historical* simulations are found over north-east South America. The dry season is important in this region due to the presence of perennial vegetation (forest and cocoa crops), which are influenced by dry season climate, as well as wet season climate. Drier dry seasons may be detrimental to forest survival in this region (McDowell et al., 2018). Therefore this region is considered in more detail.

3.2. Dry Season Changes Over North-East South America

Links between dry spell duration and global climatic indices are now investigated in detail over north-east South America to assess the physical consistency of driving mechanisms between present day and future changes.

3.2.1. Role of SST Variability in Dry Spell Trend

The mean length of dry spells in the dry season over north-east South America (Figure 2a) is correlated with SSTs averaged over the dry season (taken as May-September, Figure 3a). Two distinct patterns are apparent. The first is a positive correlation between tropical North Atlantic SSTs (roughly 0–20°N, 20–70°W), and stronger in the west than in the east. Individual month correlations for May-September (not shown) suggest that this positive correlation is strongest in the early dry season and weakens throughout the boreal summer (though still present in September). The second pattern is a negative correlation with central and eastern equatorial Pacific SSTs; this pattern resembles an ENSO SST pattern. This correlation pattern strengthens as the dry season progresses (not

Figure 2. Timeseries of mean length of dry spells in the dry season over a) South America, c) West Africa and the Sahel and e) Southern Africa from Climate Hazards group Infrared Precipitation with Stations and ERA5 and the mean over 20 *amip* simulations. Anomalies are computed using the mean for the whole period. Boxplots show the range of trends from observations, *historical*, *amip*, and *hist-nat* simulations over a) South America, c) West Africa and the Sahel and e) Southern Africa. For *amip* and *historical* the boxplot shows the range of values for the 10 models for which daily precipitation was available for *hist-nat*; the gray shaded line shows the range (excluding outliers) across all 20 models. The box extends from the lower quartile (Q1) to the upper quartile (Q3) of the data and the line (cross) in the middle shows the median (mean). The whiskers extend from the first datum greater than Q1 minus 1.5 times the interquartile range to the last datum less than Q3 plus 1.5 times the interquartile range - values outside this range are considered to be outliers and marked with a circle. g) Mean May-September (dry season over South America) Atlantic Multi-Decadal Oscillation (AMO) and El-Niño Southern Oscillation (ENSO) indices.

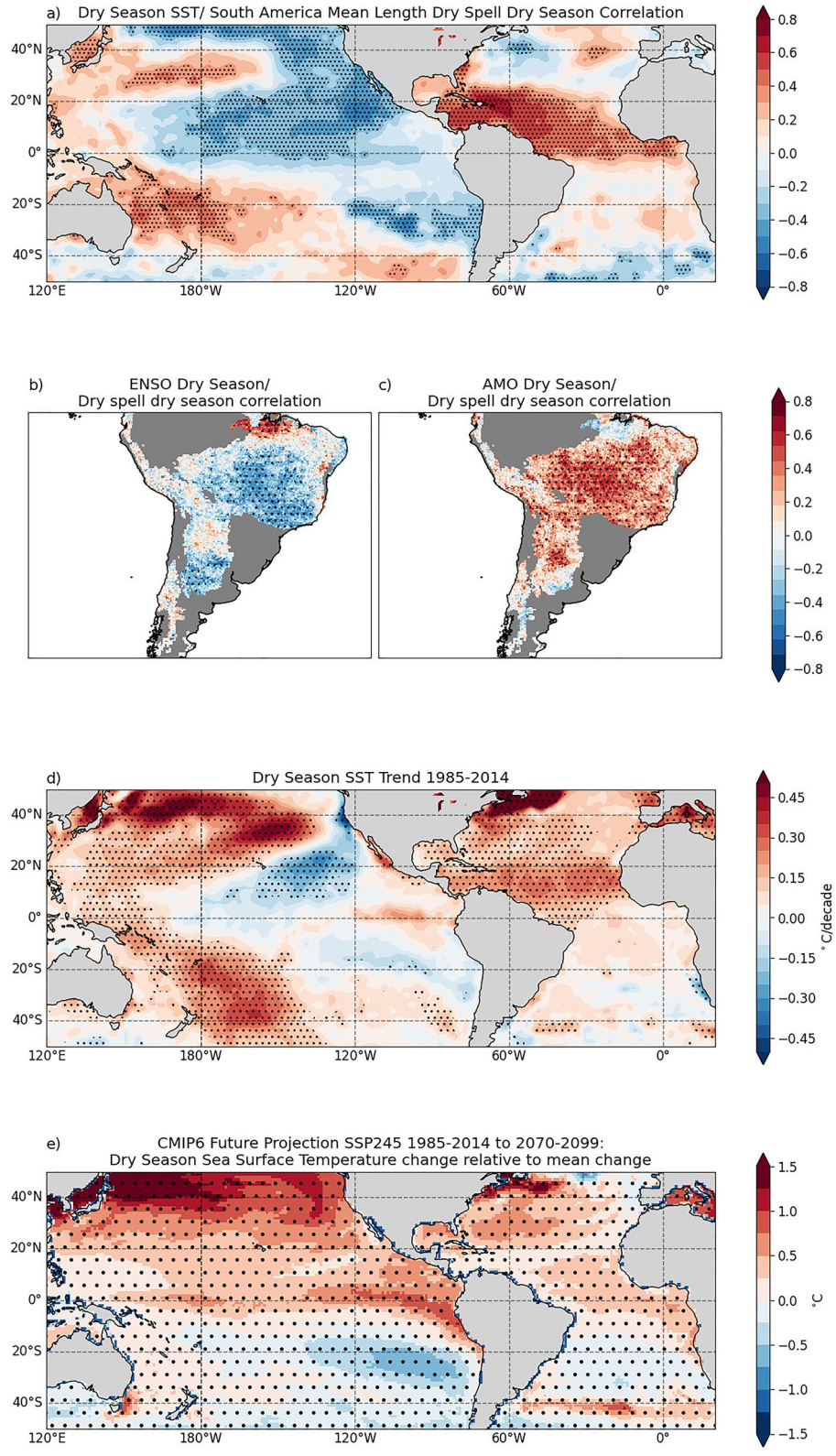

Figure 3.

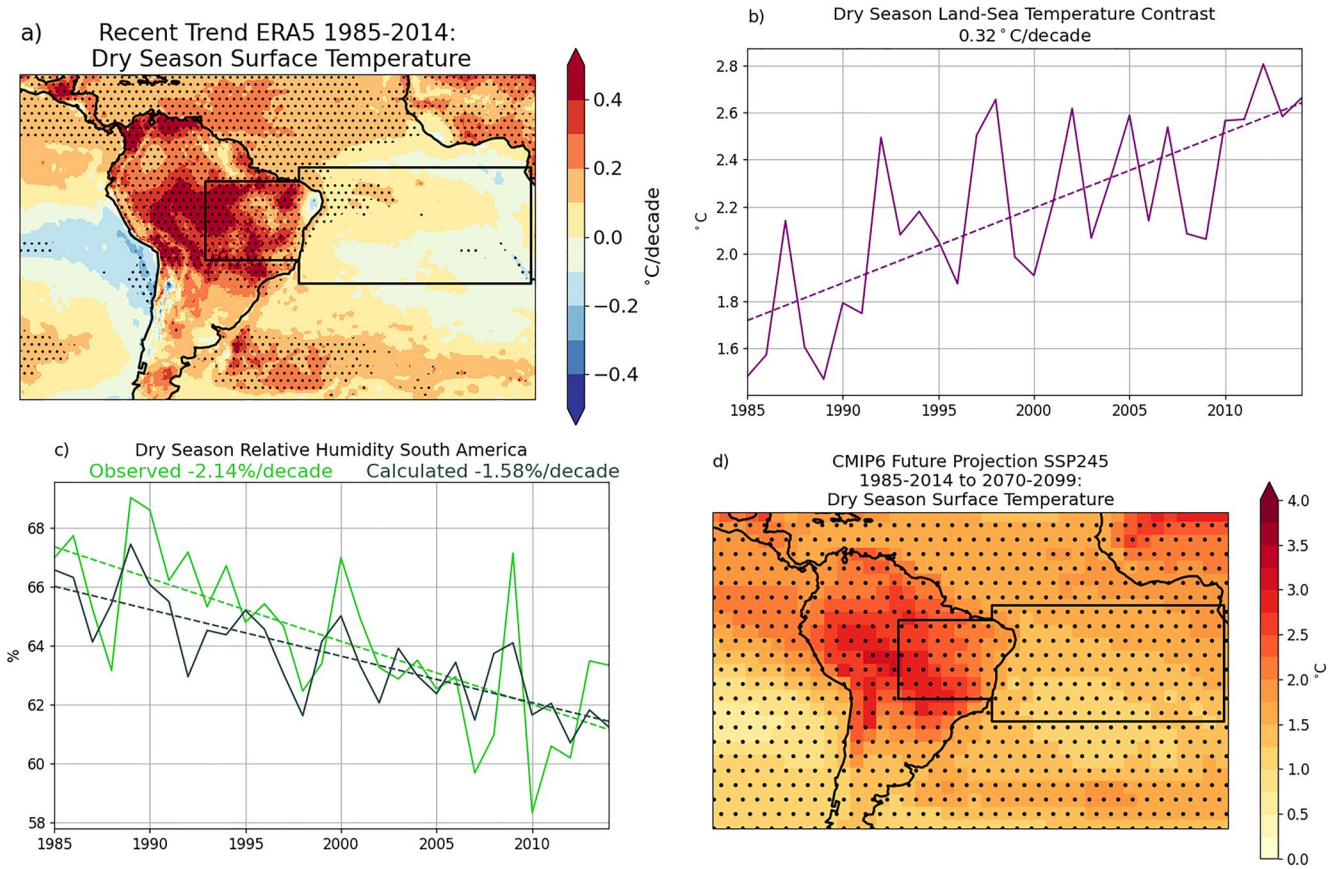

Figure 4. (a) Trend in dry season (May-September) surface temperature from ERA5 over 1985-2014; stippling indicates statistical significance at the 10% level. The regions used for the land and sea region are marked. (b) Timeseries of dry season land-sea temperature contrast and trend line; land-sea temperature contrast was calculated by taking the difference of the land and sea regions shown in (a). (c) Observed and calculated dry season relative humidity over the land region and trend line; calculated relative humidity uses specific humidity from the sea region and saturated specific humidity from the land region. (d) Multi-model median change in dry season surface temperature from 20 Coupled Model Intercomparison Project phase 6 models comparing 2070-2099 under Shared Socioeconomic Pathway 245 with 1985-2014 under the *historical* scenario. Robust changes (see Section 2.4) are stippled.

shown), with a characteristic oppositely correlated horseshoe pattern in the western Pacific present from June/July onwards. Mean dry season ENSO and AMO indices were correlated with the mean length of dry spells in the dry season at each grid point; the AMO shows a strong positive correlation across South America (Figure 3c), while the ENSO correlation exhibits a negative correlation (Figure 3b).

Figures 3a and 3c suggests the longer dry spells in the dry season over north-east South America are related to warm SSTs in the tropical North Atlantic, especially at the beginning of the dry season. Warmer North Atlantic SSTs modify the northward global energy transports, resulting in a northward displacement of the tropical rainband (Hodson et al., 2022; Monerie et al., 2019), thus leading to drier conditions (and longer dry spells) during the dry season over South America. Hodson et al. (2022), Monerie et al. (2019), and Knight et al. (2006) have shown that positive AMO conditions (warm SST in the North Atlantic) are associated with dry conditions over northern South America. Figure 3d shows the warming of dry season SSTs over the tropical North Atlantic region from 1985 to 2014, and the AMO has moved from a negative to positive phase over this period (Figure 2g), suggesting that this may have contributed to the trend of longer dry season dry spells over north-east

Figure 3. (a) Correlation between the timeseries of the mean length of dry spells in the dry season over the South America region shown in Figure 1a and dry season (May-September) sea surface temperature (SSTs) from HadISST over 1986-2014. (b) Correlation between the dry season El Niño Southern Oscillation index and mean length of dry spells in the dry season at each grid point. (c) Correlation between the dry season Altantic multidecadal oscillation index and mean length of dry spells in the dry season at each grid point. For a-c stippling indicates statistical significance at the 10% level. (d) Trend in dry season (May-September) HadISST SST over 1985-2014; stippling indicates statistical significance at the 10% level. (e) Multi-model median change in dry season SST from 19 Coupled Model Intercomparison Project phase 6 models comparing 2070-2099 under Shared Socioeconomic Pathway 245 with 1985-2014 under the *historical* scenario. The change is shown relative to the multi-model mean SST change. Robust future changes relative to the present-day period (see Section 2.4) are stippled.

South America. Under future climate change, the AMO is unlikely to change its behavior (Knudsen et al., 2011; Villamayor et al., 2018), but CMIP6 projections show greater warming in the North Atlantic compared to the South Atlantic (1.4°C vs. 1.1°C), suggesting this may also be contributing to the future trend of longer dry spells in the dry season over this region.

Figures 3a and 3b also suggest that longer dry spells in the dry season over north-east South America are related to cooler SSTs in the equatorial Pacific and La Niña events. The correlation map in Figure 3a and the SST trend in Figure 3d exhibit a pattern of teleconnections that is broader in its latitude range than typically manifested by ENSO variability and may be indicative of a decadal mode variability, commonly referred to in the literature as Pacific Decadal Variability/Oscillation or Interdecadal Pacific Oscillation (Maidment et al., 2015; Villamayor et al., 2018). El Niño events are typically linked with dry conditions over South America, although most studies tend to focus on the austral summer when ENSO peaks and the annual wet season occurs over South America. Figure 3d shows a slight negative trend over this region for the period of interest, which may be linked with longer dry spells. With the future warming of the climate, the change in ENSO SST variability is highly uncertain (Fredriksen et al., 2020). CMIP6 projections show greater equatorial warming in the Pacific compared to the off-equatorial region and faster warming of the eastern compared with the west, that is, showing a more El-Niño like SST warming pattern.

3.2.2. Land-Sea Warming Contrast

Faster warming over land than the ocean, an expected consequence of a warming climate and observed over recent decades, has been linked with declining relative humidity over land (Byrne & O'Gorman, 2018). This is explained by the supply of moisture from the oceans increasing at a slower rate than the saturated vapor pressure increase over land, leading to a decline in relative humidity that can be further amplified by land-vegetation feedback (Berg et al., 2016). Figure 4a shows that over 1985–2014 surface temperatures during the dry season (May-September) increased at a faster rate over South America than over the adjacent South Atlantic, with the dry season land-sea temperature contrast increasing at a rate of 0.32°C/decade (Figure 4b).

Figure 4c compares the dry season trend in relative humidity from observations and estimated based on calculations isolating the influence of land-sea warming contrast on the supply of ocean moisture (see Section 2.5 for methodology). The estimated relative humidity decline related to land-ocean warming contrast (−1.6%/decade) is smaller than observed (−2.1%/decade) suggesting that while the land-sea warming contrast can account for about 75% of the decrease (and explains ∼60% of the year-to-year variance), other factors have also contributed. Dry season evaporation has also decreased over the region (possibly related to reduced soil moisture, Figure S3), which may also contribute to dry season drying over the region, and longer dry spells. Although there may be other oceanic and continental sources of moisture, and influence from atmospheric circulation changes (e.g., previous section), Figure 4 suggests that the relative humidity decline and drying during the dry season over South America are consistent with the rising land temperature but fairly constant ocean specific humidity.

Future projections (Figure 4d) indicate that the land will continue to warm faster than the ocean (2.3°C over land region vs. 1.5°C over the ocean region, comparing 2070-2099 under SSP245 with 1985-2014 under the *historical* scenario), contributing to a continuing relative humidity decrease (∼3% using a similar method as applied to the present day changes, see Supplementary Information), indicating that the strengthening land-ocean warming contrast also contributes to the trend of longer dry spells in the dry season under future climate change.

4. Discussion and Conclusions

We identify that recently observed trends in the mean length of dry spells in the dry season display a qualitatively consistent pattern to future projected changes for the end of the 21st century and investigate the role of natural and anthropogenic forcings and physical mechanisms common to both recent trends and future projections. The main conclusions are:

1. There are increases in dry season dry spell length of up to about 2 days per decade over north-east South America, southern North America, and southern Africa, and decreases of similar magnitude over West Africa and the Sahel during 1985–2014.
2. Anthropogenic influences have played a role in recent dry spell trends over north-east South America, and the West Africa/Sahel region.

3. Warm SSTs in the north Atlantic are associated with longer dry season dry spells over South America. Warm SSTs may lead to a more northerly position of the tropical rainband during the austral winter (Hodson et al., 2022; Monerie et al., 2019), thus leading to drier conditions (and longer dry spells) during the dry season over South America. Under future climate change, the North Atlantic is projected to warm more than the South Atlantic, suggesting this may also be contributing to the future trend of longer dry spells in the dry season over South America.
4. Changes in the land-sea warming contrast mean that the oceanic supply of moisture is insufficient to maintain relative humidity levels over land, resulting in elevated aridity and drier conditions during the dry season (Berg et al., 2016; Byrne & O'Gorman, 2018); this is also projected to continue with future climate change.

The trend of longer dry season dry spells over South America may also be influenced by deforestation. Deforestation modifies moisture recycling and decreases the latent heat flux, meaning that stronger moisture transport and deeper convection are needed to trigger rainfall (Leite-Filho et al., 2019; Llopart et al., 2018). Leite-Filho et al. (2019) found that deforestation led to a greater probability of dry spells during the early and late rainy season in Southern Amazonia, and Spracklen and Garcia-Carreras (2015) found that large-scale deforestation in the Amazon reduced rainfall totals. Continuing deforestation and changing land use in the region considered here may have contributed to changes in latent heat flux, increases in surface temperature over land (Li et al., 2016), and longer dry spells, and therefore merits further study.

The consistency between recent trends and future projected changes, along with consistent physical mechanisms for longer dry spells over north-east South America, contributes toward establishing robustness in these future responses. Further work, including crop modeling studies, should aim to establish the resultant impacts on vegetation, including perennial tree crops, to inform suitable adaptation methods to minimize the impacts of longer dry spells. In addition, detailed studies for West Africa and the Sahel, and southern Africa, are merited to explore the observed signals and drivers and inform future projections.

Data Availability Statement

Open Research CHIRPS data is available from https://www.chc.ucsb.edu/data/chirps. MSWEP data is available from http://www.gloh2o.org/mswep/. The ERA5 dataset is available from the Climate Data store: https://confluence.ecmwf.int/display/CKB/How+to+download+ERA5. HadISST data is available from https://www.metoffice.gov.uk/hadobs/hadisst/. The AMO index used is available from https://climatedataguide.ucar.edu/climate-data/atlantic-multi-decadal-oscillation-amo. The ENSO index is available from https://origin.cpc.ncep.noaa.gov/products/analysis_monitoring/ensostuff/ONI_v5.php. CMIP6 data is available from https://esgf-node.llnl.gov/projects/cmip6/.

Acknowledgments
The World Climate Research Programme Working Group on Coupled Modelling is acknowledged for coordinating CMIP6. We thank the climate modeling groups (Table S1) for producing and making available their model output, the Earth System Grid Federation (ESGF) for archiving the data and providing access, and the multiple funding agencies who support CMIP6 and ESGF. Emily Black was supported by the National Centre for Atmospheric Science via the NERC/GCRF programme Atmospheric hazard in developing countries: risk assessment and early warning (ACREW) and the Global Challenges Research Fund project, SatWIN-ALERT(NE/R014116/1). Richard P. Allan was funded by the National Centre for Earth Observation grant NE/RO16518/1. We are grateful to the Mars Wrigley Confectionery research team and Dan Hodson for stimulating discussions on the wider context and applications of this work.

References

Allan, R. P., Barlow, M., Byrne, M. P., Cherchi, A., Douville, H., Fowler, H. J., et al. (2020). Advances in understanding large-scale responses of the water cycle to climate change. *Annals of the New York Academy of Sciences*, *1472*(1), 49–75. https://doi.org/10.1111/nyas.14337

Avila-Diaz, A., Benezoli, V., Justino, F., Torres, R., & Wilson, A. (2020). Assessing current and future trends of climate extremes across Brazil based on reanalyses and Earth system model projections. *Climate Dynamics*, *55*(5), 1403–1426. https://doi.org/10.1007/s00382-020-05333-z

Bai, L., Shi, C., Li, L., Yang, Y., & Wu, J. (2018). Accuracy of CHIRPS satellite-rainfall products over mainland China. *Remote Sensing*, *10*(3), 362. https://doi.org/10.3390/rs10030362

Barry, A., Caesar, J., Klein Tank, A., Aguilar, E., McSweeney, C., Cyrille, A. M., et al. (2018). West Africa climate extremes and climate change indices. *International Journal of Climatology*, *38*, e921–e938. https://doi.org/10.1002/joc.5420

Beck, H. E., Wood, E. F., Pan, M., Fisher, C. K., Miralles, D. G., van Dijk, A. I. J. M., & Adler, R. F. (2019). MSWEP V2 global 3-hourly 0.1 precipitation: Methodology and quantitative assessment. *Bulletin of the American Meteorological Society*, *100*(3), 473–500. https://doi.org/10.1175/bams-d-17-0138.1

Berg, A., Findell, K., Lintner, B., Giannini, A., Seneviratne, S. I., van den Hurk, B., & Milly, P. C. D. (2016). Land–atmosphere feedbacks amplify aridity increase over land under global warming. *Nature Climate*, *6*(9), 869–874. https://doi.org/10.1038/nclimate3029

Bombardi, R. J., Kinter, J. L., III, & Frauenfeld, O. W. (2019). A global gridded dataset of the characteristics of the rainy and dry seasons. *Bulletin of the American Meteorological Society*, *100*(7), 1315–1328. https://doi.org/10.1175/bams-d-18-0177.1

Burton, C., Kelley, D. I., Jones, C. D., Betts, R. A., Cardoso, M., & Anderson, L. (2021). South American fires and their impacts on ecosystems increase with continued emissions. *Climate Resilience and Sustainability*, *e8*. https://doi.org/10.1002/cli2.8

Byrne, M. P., & O'Gorman, P. A. (2018). Trends in continental temperature and humidity directly linked to ocean warming. *Proceedings of the National Academy of Sciences*, *115*, 4863–4868. https://doi.org/10.1073/pnas.1722312115

Cerón, W. L., Kayano, M. T., Andreoli, R. V., Avila-Diaz, A., Ayes, I., Freitas, E. D., et al. (2021). Recent intensification of extreme precipitation events in the La Plata Basin in southern south America (1981–2018). *Atmospheric Research*, *249*. https://doi.org/10.1016/j.atmosres.2020.105299

Cook, K. H. (2001). A southern hemisphere wave response to ENSO with implications for southern Africa precipitation. *Journal of the Atmospheric Sciences*, *58*(15), 2146–2162. https://doi.org/10.1175/1520-0469(2001)058<2146:ashwrt>2.0.co;2
Correa, I. C., Arias, P. A., & Rojas, M. (2021). Evaluation of multiple indices of the South American monsoon. *International Journal of Climatology*, *41*, E2801–E2819. https://doi.org/10.1002/joc.6880
Dembélé, M., & Zwart, S. J. (2016). Evaluation and comparison of satellite-based rainfall products in Burkina Faso, West Africa. *International Journal of Remote Sensing*, *37*(17), 3995–4014. https://doi.org/10.1080/01431161.2016.1207258
Dinku, T., Funk, C., Peterson, P., Maidment, R., Tadesse, T., Gadain, H., & Ceccato, P. (2018). Validation of the CHIRPS satellite rainfall estimates over eastern Africa. *Quarterly Journal of the Royal Meteorological Society*, *144*, 292–312. https://doi.org/10.1002/qj.3244
Dong, B., & Sutton, R. (2015). Dominant role of greenhouse-gas forcing in the recovery of Sahel rainfall. *Nature Climate Change*, *5*(8), 757–760. https://doi.org/10.1038/nclimate2664
Dosio, A., Jones, R. G., Jack, C., Lennard, C., Nikulin, G., & Hewitson, B. (2019). What can we know about future precipitation in Africa? Robustness, significance and added value of projections from a large ensemble of regional climate models. *Climate Dynamics*, *53*(9), 5833–5858. https://doi.org/10.1007/s00382-019-04900-3
Dunning, C. M., Black, E. C., & Allan, R. P. (2016). The onset and cessation of seasonal rainfall over Africa. *Journal of Geophysical Research: Atmospheres*, *121*(19), 11405–11424. https://doi.org/10.1002/2016jd025428
Espinoza, J. C., Sörensson, A. A., Ronchail, J., Molina-Carpio, J., Segura, H., Gutierrez-Cori, O., & Wongchuig-Correa, S. (2019). Regional hydro-climatic changes in the southern Amazon basin (upper Madeira basin) during the 1982–2017 period. *Journal of Hydrology: Regional Studies*, *26*, 100637. https://doi.org/10.1016/j.ejrh.2019.100637
Eyring, V., Bony, S., Meehl, G. A., Senior, C. A., Stevens, B., Stouffer, R. J., & Taylor, K. E. (2016). Overview of the coupled model intercomparison project phase 6 (CMIP6) experimental design and organization. *Geoscientific Model Development*, *9*(5), 1937–1958. https://doi.org/10.5194/gmd-9-1937-2016
Feng, X., Porporato, A., & Rodriguez-Iturbe, I. (2013). Changes in rainfall seasonality in the tropics. *Nature Climate Change*, *3*(9), 811–815. https://doi.org/10.1038/nclimate1907
Fischer, E. M., & Knutti, R. (2016). Observed heavy precipitation increase confirms theory and early models. *Nature Climate Change*, *6*(11), 986–991. https://doi.org/10.1038/nclimate3110
Fredriksen, H.-B., Berner, J., Subramanian, A. C., & Capotondi, A. (2020). How does El Niño–Southern Oscillation change under global warming—A first look at CMIP6. *Geophysical Research Letters*, *47*(22), e2020GL090640. https://doi.org/10.1029/2020gl090640
Funk, C., Peterson, P., Landsfeld, M., Pedreros, D., Verdin, J., Shukla, S., et al. (2015). The climate hazards infrared precipitation with stations—A new environmental record for monitoring extremes. *Scientific Data*, *2*(1), 1–21. https://doi.org/10.1038/sdata.2015.66
Gillett, N. P., Shiogama, H., Funke, B., Hegerl, G., Knutti, R., Matthes, K., & Tebaldi, C. (2016). The detection and attribution model intercomparison project (DAMIP v1. 0) contribution to CMIP6. *Geoscientific Model Development*, *9*(10), 3685–3697. https://doi.org/10.5194/gmd-9-3685-2016
Gimeno, L., Drumond, A., Nieto, R., Trigo, R. M., & Stohl, A. (2010). On the origin of continental precipitation. *Geophysical Research Letters*, *37*(13), L13804. https://doi.org/10.1029/2010gl043712
Giorgi, F., Raffaele, F., & Coppola, E. (2019). The response of precipitation characteristics to global warming from climate projections. *Earth System Dynamics*, *10*(1), 73–89. https://doi.org/10.5194/esd-10-73-2019
Greve, P., & Seneviratne, S. I. (2015). Assessment of future changes in water availability and aridity. *Geophysical Research Letters*, *42*(13), 5493–5499. https://doi.org/10.1002/2015gl064127
Gupta, V., Jain, M. K., Singh, P. K., & Singh, V. (2020). An assessment of global satellite-based precipitation datasets in capturing precipitation extremes: A comparison with observed precipitation dataset in India. *International Journal of Climatology*, *40*(8), 3667–3688. https://doi.org/10.1002/joc.6419
Hersbach, H., Bell, B., Berrisford, P., Hirahara, S., Horányi, A., Muñoz-Sabater, J., et al. (2020). The ERA5 global reanalysis. *Quarterly Journal of the Royal Meteorological Society*, *146*(730), 1999–2049. https://doi.org/10.1002/qj.3803
Hodson, D. L. R., Bretonnière, P.-A., Cassou, C., Davini, P., Klingaman, N. P., Lohmann, K., et al. (2022). Coupled climate response to Atlantic Multidecadal Variability in a multi-model multi-resolution ensemble. *Climate Dynamics*. https://doi.org/10.1007/S00382-022-06157-9
Knight, J. R., Folland, C. K., & Scaife, A. A. (2006). Climate impacts of the Atlantic multidecadal oscillation. *Geophysical Research Letters*, *33*(17), L17706. https://doi.org/10.1029/2006gl026242
Knudsen, M. F., Seidenkrantz, M.-S., Jacobsen, B. H., & Kuijpers, A. (2011). Tracking the Atlantic multidecadal oscillation through the last 8,000 years. *Nature Communications*, *2*(1), 1–8. https://doi.org/10.1038/ncomms1186
Konapala, G., Mishra, A. K., Wada, Y., & Mann, M. E. (2020). Climate change will affect global water availability through compounding changes in seasonal precipitation and evaporation. *Nature Communications*, *11*, 3044. https://doi.org/10.1038/s41467-020-16757-w
Kosaka, Y., & Xie, S.-P. (2013). Recent global-warming hiatus tied to equatorial Pacific surface cooling. *Nature*, *501*(7467), 403–407. https://doi.org/10.1038/nature12534
Leite-Filho, A. T., de Sousa Pontes, V. Y., & Costa, M. H. (2019). Effects of deforestation on the onset of the rainy season and the duration of dry spells in southern Amazonia. *Journal of Geophysical Research: Atmospheres*, *124*(10), 5268–5281.
Li, Y., Zhao, M., Mildrexler, D. J., Motesharrei, S., Mu, Q., Kalnay, E., & Wang, K. (2016). Potential and actual impacts of deforestation and afforestation on land surface temperature. *Journal of Geophysical Research: Atmospheres*, *121*(24), 14–372. https://doi.org/10.1002/2016jd024969
Liebmann, B., Bladé, I., Kiladis, G. N., Carvalho, L. M., Senay, B. G., Allured, D., & Funk, C. (2012). Seasonality of African precipitation from 1996 to 2009. *Journal of Climate*, *25*(12), 4304–4322. https://doi.org/10.1175/jcli-d-11-00157.1
Liu, C., & Allan, R. P. (2013). Observed and simulated precipitation responses in wet and dry regions 1850-2100. *Environmental Research Letters*, *8*. https://doi.org/10.1088/1748-9326/8/3/034002
Llopart, M., Reboita, M. S., Coppola, E., Giorgi, F., Da Rocha, R. P., & De Souza, D. O. (2018). Land use change over the Amazon Forest and its impact on the local climate. *Water*, *10*(2), 149. https://doi.org/10.3390/w10020149
Maidment, R. I., Allan, R. P., & Black, E. (2015). Recent observed and simulated changes in precipitation over Africa. *Geophysical Research Letters*, *42*, 8155–8164. https://doi.org/10.1002/2015GL065765
Mamalakis, A., Randerson, J. T., Yu, J.-Y., Pritchard, M. S., Magnusdottir, G., Smyth, P., & Foufoula-Georgiou, E. (2021). Zonally contrasting shifts of the tropical rain belt in response to climate change. *Nature Climate Change*, *11*(2), 143–151. https://doi.org/10.1038/s41558-020-00963-x
McDowell, N., Allen, C. D., Anderson-Teixeira, K., Brando, P., Brienen, R., Chambers, J., et al. (2018). Drivers and mechanisms of tree mortality in moist tropical forests. *New Phytologist*, *219*(3), 851–869. https://doi.org/10.1111/nph.15027
Mitchell, D. M., Lo, Y. E., Seviour, W. J., Haimberger, L., & Polvani, L. M. (2020). The vertical profile of recent tropical temperature trends: Persistent model biases in the context of internal variability. *Environmental Research Letters*, *15*(10), 1040b4. https://doi.org/10.1088/1748-9326/ab9af7

Monerie, P.-A., Robson, J., Dong, B., Hodson, D. L., & Klingaman, N. P. (2019). Effect of the Atlantic multidecadal variability on the global monsoon. *Geophysical Research Letters*, *46*(3), 1765–1775. https://doi.org/10.1029/2018gl080903

New, M., Hewitson, B., Stephenson, D. B., Tsiga, A., Kruger, A., Manhique, A., et al. (2006). Evidence of trends in daily climate extremes over southern and west Africa. *Journal of Geophysical Research*, *111*(D14). https://doi.org/10.1029/2005jd006289

O'Neill, B. C., Tebaldi, C., van Vuuren, D. P., Eyring, V., Friedlingstein, P., Hurtt, G., & Sanderson, B. M. (2016). The scenario model intercomparison project (ScenarioMIP) for CMIP6. *Geoscientific Model Development*, *9*(9), 3461–3482.

Padrón, R. S., Gudmundsson, L., Decharme, B., Ducharne, A., Lawrence, D. M., Mao, J., & Seneviratne, S. I. (2020). Observed changes in dry season water availability attributed to human-induced climate change. *Nature Geoscience*, *13*(7), 477–481. https://doi.org/10.1038/s41561-020-0594-1

Paredes-Trejo, F. J., Barbosa, H., & Kumar, T. L. (2017). Validating CHIRPS-based satellite precipitation estimates in Northeast Brazil. *Journal of Arid Environments*, *139*, 26–40. https://doi.org/10.1016/j.jaridenv.2016.12.009

Pascale, S., Lucarini, V., Feng, X., Porporato, A., & ul Hasson, S. (2016). Projected changes of rainfall seasonality and dry spells in a high greenhouse gas emissions scenario. *Climate Dynamics*, *46*, 1331–1350. https://doi.org/10.1007/s00382-015-2648-4

Rayner, N., Parker, D. E., Horton, E., Folland, C. K., Alexander, L. V., Rowell, D., & Kaplan, A. (2003). Global analyses of sea surface temperature, sea ice, and night marine air temperature since the late nineteenth century. *Journal of Geophysical Research*, *108*(D14), 4407. https://doi.org/10.1029/2002jd002670

Rivera, J. A., Marianetti, G., & Hinrichs, S. (2018). Validation of CHIRPS precipitation dataset along the central Andes of Argentina. *Atmospheric Research*, *213*, 437–449. https://doi.org/10.1016/j.atmosres.2018.06.023

Schurer, A. P., Ballinger, A. P., Friedman, A. R., & Hegerl, G. C. (2020). Human influence strengthens the contrast between tropical wet and dry regions. *Environmental Research Letters*, *15*, 104026. https://doi.org/10.1088/1748-9326/ab83ab

Seneviratne, S. I., Nicholls, N., Easterling, D., Goodess, C., Kanae, S., & Kossin, J., (2012). Changes in climate extremes and their impacts on the natural physical environment. In *Managing the risks of extreme events and disasters to advance climate change adaptation* (pp. 109–230). A Special Report of Working Groups I and II of the Intergovernmental Panel on Climate Change (IPCC). Cambridge University Press.

Shen, Z., Yong, B., Gourley, J. J., Qi, W., Lu, D., Liu, J., & Zhang, J. (2020). Recent global performance of the climate hazards group infrared precipitation (CHIRP) with stations (CHIRPS). *Journal of Hydrology*, *591*, 125284. https://doi.org/10.1016/j.jhydrol.2020.125284

Sillmann, J., Kharin, V., Zhang, X., Zwiers, F., & Bronaugh, D. (2013). Climate extremes indices in the CMIP5 multimodel ensemble: Part 1. Model evaluation in the present climate. *Journal of Geophysical Research: Atmospheres*, *118*(4), 1716–1733. https://doi.org/10.1002/jgrd.50203

Sillmann, J., Kharin, V. V., Zwiers, F., Zhang, X., & Bronaugh, D. (2013). Climate extremes indices in the CMIP5 multimodel ensemble: Part 2. Future climate projections. *Journal of Geophysical Research: Atmospheres*, *118*(6), 2473–2493. https://doi.org/10.1002/jgrd.50188

Slette, I. J., Blair, J. M., Fay, P. A., Smith, M. D., & Knapp, A. K. (2021). Effects of compounded precipitation pattern intensification and drought occur belowground in a Mesic grassland. *Ecosystems*. https://doi.org/10.1007/s10021-021-00714-9

Spracklen, D., & Garcia-Carreras, L. (2015). The impact of Amazonian deforestation on Amazon basin rainfall. *Geophysical Research Letters*, *42*(21), 9546–9552. https://doi.org/10.1002/2015gl066063

Tierney, J. E., Ummenhofer, C. C., & DeMenocal, P. B. (2015). Past and future rainfall in the Horn of Africa. *Science Advances*, *1*(9), e1500682. https://doi.org/10.1126/sciadv.1500682

Toté, C., Patricio, D., Boogaard, H., Van der Wijngaart, R., Tarnavsky, E., & Funk, C. (2015). Evaluation of satellite rainfall estimates for drought and flood monitoring in Mozambique. *Remote Sensing*, *7*(2), 1758–1776. https://doi.org/10.3390/rs70201758

Trenberth, K., & Shea, D. (2006). Atlantic hurricanes and natural variability in 2005. *Geophysical Research Letters*, *33*(12), L12704. https://doi.org/10.1029/2006gl026894

Trenberth, K., Zhang, R., & for Atmospheric-Research-Staff, N.-C. (2021). *The climate data guide: Atlantic multi-decadal oscillation (amo)*. Retrieved from https://climatedataguide.ucar.edu/climate-data/atlantic-multi-decadal-oscillation-amo

Valverde, M. C., & Marengo, J. A. (2014). Extreme rainfall indices in the hydrographic basins of Brazil. *Open Journal of Modern Hydrology*, *4*(1), 10–26. https://doi.org/10.4236/ojmh.2014.41002

Vicente-Serrano, S. M., McVicar, T. R., Miralles, D. G., Yang, Y., & Tomas-Burguera, M. (2020). Unraveling the influence of atmospheric evaporative demand on drought and its response to climate change. *Wiley Interdisciplinary Reviews: Climate Change*, *11*, e632. https://doi.org/10.1002/wcc.632

Villamayor, J., Ambrizzi, T., & Mohino, E. (2018). Influence of decadal sea surface temperature variability on northern Brazil rainfall in CMIP5 simulations. *Climate Dynamics*, *51*(1), 563–579. https://doi.org/10.1007/s00382-017-3941-1

Wainwright, C. M., Black, E., & Allan, R. P. (2021). Future changes in wet and dry season characteristics in CMIP5 and CMIP6 simulations. *Journal of Hydrometeorology*, *22*(9), 2339–2357. https://doi.org/10.1175/JHM-D-21-0017.1

Watters, D., Battaglia, A., & Allan, R. P. (2021). The diurnal cycle of precipitation according to multiple decades of global satellite observations, three CMIP6 models, and the ECMWF reanalysis. *Journal of Climate*, *34*(12), 5063–5080. https://doi.org/10.1175/jcli-d-20-0966.1

Wood, G. A. R., & Lass, R. (2008). *Cocoa*. John Wiley & Sons.

Zhang, W., Brandt, M., Tong, X., Tian, Q., & Fensholt, R. (2018). Impacts of the seasonal distribution of rainfall on vegetation productivity across the Sahel. *Biogeosciences*, *15*, 319–330. https://doi.org/10.5194/bg-15-319-2018

Zilli, M. T., Carvalho, L. M., & Lintner, B. R. (2019). The poleward shift of South Atlantic Convergence Zone in recent decades. *Climate Dynamics*, *52*(5), 2545–2563.

Zuidema, P. A., Babst, F., Groenendijk, P., Trouet, V., Abiyu, A., Acuña-Soto, R., et al. (2022). Tropical tree growth driven by dry-season climate variability. *Nature Geoscience*, *15*, 269–276.

References From the Supporting Information

Bi, D., Dix, M., Marsland, S., O'Farrell, S., Sullivan, A., Bodman, R., et al. (2020). Configuration and spin-up of ACCESS-CM2, the new generation Australian community climate and Earth system simulator coupled model. *Journal of Southern Hemisphere Earth Systems Science*, *70*(1), 225–251. https://doi.org/10.1071/es19040

Boucher, O., Servonnat, J., Albright, A. L., Aumont, O., Balkanski, Y., Bastrikov, V., & Vuichard, N. (2020). Presentation and evaluation of the IPSL-CM6A-LR climate model. *Journal of Advances in Modeling Earth Systems*, *12*(7), e2019MS002010. https://doi.org/10.1029/2019MS002010

Cao, J., Wang, B., Yang, Y.-M., Ma, L., Li, J., Sun, B., & Wu, L. (2018). The NUIST Earth system model (NESM) version 3: Description and preliminary evaluation. *Geoscientific Model Development*, *11*(7), 2975–2993. https://doi.org/10.5194/gmd-11-2975-2018

Dunne, J., Horowitz, L., Adcroft, A., Ginoux, P., Held, I., John, J., et al. (2020). The GFDL Earth System Model version 4.1 (GFDL-ESM 4.1): Overall coupled model description and simulation characteristics. *Journal of Advances in Modeling Earth Systems*, *12*(11), e2019MS002015. https://doi.org/10.1029/2019ms002015

Gettelman, A., Hannay, C., Bacmeister, J. T., Neale, R. B., Pendergrass, A. G., Danabasoglu, G., & Mills, M. J. (2019). High climate sensitivity in the community Earth system model version 2 (CESM2). *Geophysical Research Letters*, *46*(14), 8329–8337. https://doi.org/10.1029/2019GL083978

Gettelman, A., Mills, M., Kinnison, D., Garcia, R., Smith, A., Marsh, D., et al. (2019). The whole atmosphere community climate model version 6 (WACCM6). *Journal of Geophysical Research: Atmospheres*, *124*(23), 12380–12403. https://doi.org/10.1029/2019jd030943

Held, I., Guo, H., Adcroft, A., Dunne, J., Horowitz, L., Krasting, J., et al. (2019). Structure and performance of GFDL's CM4. 0 climate model. *Journal of Advances in Modeling Earth Systems*, *11*(11), 3691–3727. https://doi.org/10.1029/2019ms001829

Mauritsen, T., Bader, J., Becker, T., Behrens, J., Bittner, M., Brokopf, R., et al. (2019). Developments in the MPI-M Earth System Model version 1.2 (MPI-ESM1. 2) and its response to increasing CO_2. *Journal of Advances in Modeling Earth Systems*, *11*(4), 998–1038. https://doi.org/10.1029/2018ms001400

Müller, W. A., Jungclaus, J. H., Mauritsen, T., Baehr, J., Bittner, M., Budich, R., et al. (2018). A higher-resolution version of the Max Planck institute Earth system model (MPI-ESM1. 2-HR). *Journal of Advances in Modeling Earth Systems*, *10*(7), 1383–1413. https://doi.org/10.1029/2017ms001217

Pu, Y., Liu, H., Yan, R., Yang, H., Xia, K., Li, Y., et al. (2020). CAS FGOALS-g3 model datasets for the CMIP6 scenario model intercomparison project (ScenarioMIP). *Advances in Atmospheric Sciences*, *37*(10), 1081–1092. https://doi.org/10.1007/s00376-020-2032-0

Séférian, R., Delire, C., Decharme, B., Voldoire, A., Salas y Melia, D., Chevallier, M., & Sénési, S. (2016). Development and evaluation of CNRM Earth system model—CNRM-ESM1. *Geoscientific Model Development*, *9*(4), 1423–1453. https://doi.org/10.5194/gmd-9-1423-2016

Séférian, R., Nabat, P., Michou, M., Saint-Martin, D., Voldoire, A., Colin, J., & Madec, G. (2019). Evaluation of CNRM Earth system model, CNRM-ESM2-1: Role of Earth system processes in present-day and future climate. *Journal of Advances in Modeling Earth Systems*, *11*(12), 4182–4227. https://doi.org/10.1029/2019MS001791

Seland, Ø., Bentsen, M., Olivié, D., Toniazzo, T., Gjermundsen, A., Graff, L. S., & Schulz, M. (2020). Overview of the Norwegian Earth System Model (NorESM2) and key climate response of CMIP6 DECK, historical, and scenario simulations. *Geoscientific Model Development*, *13*(12), 6165–6200. https://doi.org/10.5194/gmd-13-6165-2020

Sellar, A. A., Jones, C. G., Mulcahy, J. P., Tang, Y., Yool, A., Wiltshire, A., et al. (2019). UKESM1: Description and evaluation of the UK Earth system model. *Journal of Advances in Modeling Earth Systems*, *11*(12), 4513–4558. https://doi.org/10.1029/2019ms001739

Song, Y. H., Nashwan, M. S., Chung, E.-S., & Shahid, S. (2021). Advances in CMIP6 INM-CM5 over CMIP5 INM-CM4 for precipitation simulation in South Korea. *Atmospheric Research*, *247*, 105261. https://doi.org/10.1016/j.atmosres.2020.105261

Swaminathan, R., Parker, R. J., Jones, C. G., Allan, R. P., Quaife, T., Kelley, D. I., & Walton, J. (2021). The physical climate at global warming thresholds as seen in the UK Earth system model. *Journal of Climate*, *35*(1), 1–64. https://doi.org/10.1175/JCLI-D-21-0234.1

Swart, N. C., Cole, J. N. S., Kharin, V. V., Lazare, M., Scinocca, J. F., Gillett, N. P., & Winter, B. (2019). The Canadian Earth system model version 5 (canESM5.0.3). *Geoscientific Model Development*, *12*(11), 4823–4873. https://doi.org/10.5194/gmd-12-4823-2019

Tatebe, H., Ogura, T., Nitta, T., Komuro, Y., Ogochi, K., Takemura, T., & Kimoto, M. (2019). Description and basic evaluation of simulated mean state, internal variability, and climate sensitivity in miroc6. *Geoscientific Model Development*, *12*(7), 2727–2765. https://doi.org/10.5194/gmd-12-2727-2019

Volodin, E. M., Mortikov, E. V., Kostrykin, S. V., Galin, V. Y., Lykossov, V. N., Gritsun, A. S., et al. (2018). Simulation of the modern climate using the INM-CM48 climate model. *Russian Journal of Numerical Analysis and Mathematical Modelling*, *33*(6), 367–374. https://doi.org/10.1515/rnam-2018-0032

Wu, T., Lu, Y., Fang, Y., Xin, X., Li, L., Li, W., & Liu, X. (2019). The Beijing climate center climate system model (BCC-CSM): The main progress from CMIP5 to CMIP6. *Geoscientific Model Development*, *12*(4), 1573–1600. https://doi.org/10.5194/gmd-12-1573-2019

Yukimoto, S., Kawai, H., Koshiro, T., Oshima, N., Yoshida, K., Urakawa, S., & Ishii, M. (2019). The meteorological research institute Earth system model version 2.0, MRI-ESM2.0: Description and basic evaluation of the physical component. *Journal of the Meteorological Society of Japan. Series II*, *97*(5), 931–965. https://doi.org/10.2151/jmsj.2019-051

Ziehn, T., Chamberlain, M. A., Law, R. M., Lenton, A., Bodman, R. W., Dix, M., & Srbinovsky, J. (2020). The Australian Earth system model: ACCESS-ESM1.5. *Journal of Southern Hemisphere Earth Systems Sciences*, *70*(1), 193. https://doi.org/10.1071/es19035